IJRCS

International Journal of Robotics and Control Systems
Vol. 4, No. 3, 2024, pp. 1263-1278
ISSN 2775-2658
http://pubs2.ascee.org/index.php/ijrcs

ASCEE

Design and Implementation of Crowbar and STATCOM for Enhanced Stability of Grid-Tied Doubly Fed Induction Wind Generators

Mohamed F. Elnaggar [a,b,1,*]

[a] Department of Electrical Engineering, College of Engineering, Prince Sattam Bin Abdulaziz University, Al-Kharj 11942, Saudi Arabia
[b] Department of Electrical Power and Machines Engineering, Faculty of Engineering, Helwan University, Helwan 11795, Egypt
[1] mfelnaggar@yahoo.com
* Corresponding Author

ARTICLE INFO

Article history
Received May 27, 2024
Revised July 04, 2024
Accepted July 27, 2024

Keywords
Grid Faults;
Transient Behavior;
Control Strategy;
MATLAB Simulation;
Clean Energy

ABSTRACT

These days, one of the most used layouts in the wind power industry is a variable-speed doubly-fed induction wind generator (DFIWG). For providing active power (P) and reactive power (Q) control during grid failures, this research examines the DFIWG. The system's transient behavior is examined under normal and abnormal circumstances. Through control of rotor side (RSC) and grid side (GSC) converters, Q assistance for the grid, and power converter stress reduction, the suggested control approach achieves system stability while enabling DFIWG to operate smoothly during grid failures. The DFIWG is exposed to three- and two-phase faults to analyze the machine's performance. The crowbar and STATCOM tools are implemented to enhance the system performance under faults and compared with the base case. The implemented tools successfully suppress rotor and stator overcurrent, over voltage at the DC link (DCL), and power oscillations, as well as supporting the grid voltage understudied cases. The obtained results prove that both STATCOM and crowbar not only enhance the system's effectiveness and performance but also enable the system to achieve the fault ride-through capacity (FRTC). MATLAB/SIMULINK 2017b is used for time-domain computer simulations.

1. Introduction

Doubly-fed induction wind generators (DFIWGs) have been exposed to grid disruptions when they were directly connected, via lengthy transmission lines (TLs), to the grid at near-to-ground voltages. In grids, imbalanced grid voltages (GVs) are the most prevalent. Unequal GV drops on TLs or unstable loads linked at the point of common connection (POCC) can cause imbalanced GV [1]-[4]. As a result, key grid codes were distributed by energy system operators, mandating that DFIWGs be bright to sustain a 2% and 4% for steady-state and short-term, respectively disproportion in GV without triggering [5]-[8]. Negative sequence stator/rotor current parts are produced by an imbalanced GV. There will be strong fluctuations in DCL voltage (DCLV\V_{DC}), torque, and power at twofold supply frequency. Consequently, an imbalanced generator voltage can damage generator

bearings, DCL capacitors, and DC/AC inverters. To solve these issues with no disconnecting the generating systems, the DFIWG controller systems must handle these conditions [9]-[11]. GSCs are meticulous to adjust DCLV and total Q supplied to the network, while RSCs are managed to fine-tune stator P and Q.

Numerous control systems, for instance vector (VC) and direct power (DPC) control, are investigated to regulate DFIWG in a typical setting [12], [13]. One of the favored control strategies was the DPC of DFIWG. When weighed against VC, DPC offers a number of benefits, including ease and quick response time [14]. Under uneven and deformed GV, the functioning of DPC was investigated [15].

RSC-based DPC was controlled by PI resonant controllers (PIRs) in [16]. In order to accomplish various control objectives, a power adjustment method (PAM) was included. To obtain the (+ and - sequence) parts of GV and current, nevertheless the stator deconstruction method is necessary. A static target framework DPC-based sliding mode (SM) regulator with a PAM was developed [17]. A vector-PI (VPI) controller was developed in [18] to enhance the DPC of DFIWG in the presence of harmonic GV. Synchronous relative frame implementation was used for the regulator. DPC and a separated framework for DFIWG that utilizes lagging control were coupled in [15]. Tests are conducted on the suggested controller's functionality in both symmetric GV dip and typical circumstances. Rather than employing traditional immediate power elements, the DPC method was constructed in [19] utilizing expanded concepts of P. A second-order (SO) generalized integrator (GI) was cast-off to estimate the delayed values and filtered stator voltage. DPC employs frequency adaptive vector PI (FAVPI) in [20] to lessen the impact of harmoniously and imbalanced GV. DAVPI requires an axis conversion and a frequency estimation. A voltage-modulating DPC (VM-DPC) was proposed in [21] to enhance both intermittent and constant-state performance in balance GV scenarios. An additional parallel adjuster is intended to work in tandem with the VM-DPC to regulate (-sequence) current and enhance stator current, P, and Q. Nonetheless, the gathering of the voltage and current elements of a stator in (+ and - sequence) was necessary. Ref. [22] uses extended P to build an SM-DPC approach for DFIWG.

In [23], the MP-DPC of RSC under unbalanced GV is examined. Moreover, observations of the rotor current (RC) were necessary for the computation of the rotor voltage (RV) vector. A unified PAM was suggested for a low complexity MP-DPC that was designed in [24], [25]. MP-based RC control for matrix converters was designed in [26]. RV vectors were delivered in [26] during a predetermined sample interval. On the other hand, there might be a rise in shift frequency and losses.

PI regulators have been made to function well both in abrupt and stable conditions when it comes to electrical control. Nonetheless, there are two grid frequency (GF) fluctuation elements when the grid is out of sync. Because of the inadequate gain at two times GF, PIR would not be suitable [16], [27]. To address the shortcomings of PIR, PIR was proposed [28]. PIR has the potential to attain nil steady-state error; however, the pole distribution of the control object DFIWG may cause an unanticipated peak in magnitude response at a GF greater than the resonant frequency, which is destructive to constant closed-loop (CL) process [29], [30]. Precise AC pulse monitoring and sufficient CL phase tolerance are features of the PIR. PIR can be built to eliminate the DFIWG stator P and Q pulsation components built on pole-zero annulment to prevent the surprise advance spike [29].

The performance study of DFIWG to the weak grid is examined in this research. For preventing the axial transformation of stator voltage and current, RSC regulation is built on a stationary reference frame. Equations for electromagnetic torque and stator power are derived using rotor flux under balance and imbalanced GV as inputs. To assess the DFIWG's performance, it is used with a crowbar, a FACTS device, and no additional tools. Simulation outcomes are analyzed and investigated for assessing DFIWG's performance. The performance of several approaches is assessed under balanced and unbalanced GV.

2. Description, Mathematical Modeling, and Control of the Investigated System

2.1. System Description

A back-to-back converter (BTBC) structure based on voltage source converter (VSC) has been castoff for DFIWG, and it's called by this name because of it has two parts (stator and rotor) can supply power. For grid-connected DFIWG, the stator is straight linked to the network, and the rotor is linked to the network via BTBC. The VSC of the rotor involves of two components, the RSC and GSC, which are regulated autonomously [31]-[33].

RSC is utilized to provide the required magnetizing current in the rotor winding for controlling P and Q which flow from the stator terminals of DFIWG to the network. The GSC's chief mission is to preserve the DCLV fixed. The DFIWG permits a variable speed process at (+/ -) 30% around the synchronous speed. Thus, the power movement in the rotor system is bidirectional. This necessitates a 4-quadrant VSC as given away in Fig. 1. Nevertheless, the VSC requirements to work only $\pm$ 30% of the rated value. The usage of lower-capacity VSCs outcomes in a low price, weight, and physical size as well [34]-[36].

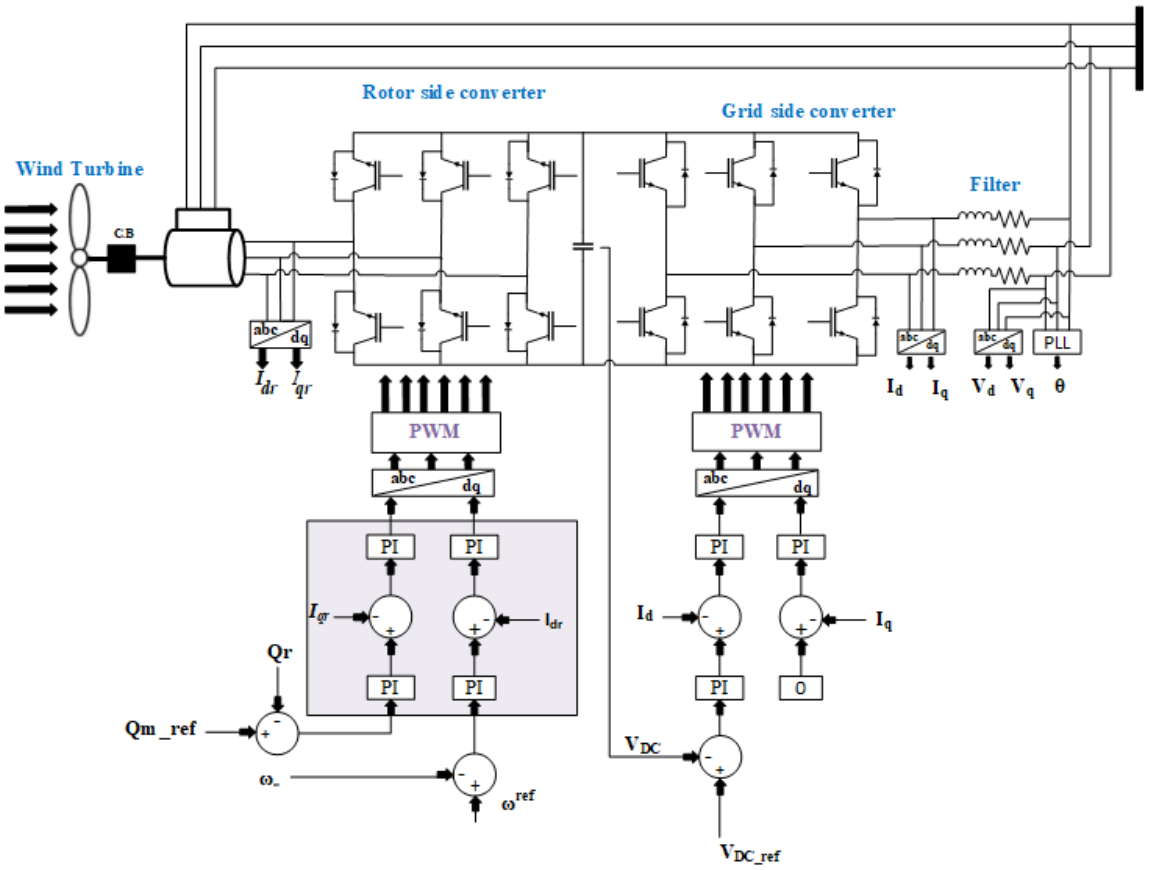

Fig. 1. Addressed grid-tied DFIWG

2.2. Mathematical Model

A mathematical model of DFIWG in a dq frame reference is recognized. The GV-oriented VC is cast-off for GSC to keep a persistent DCLV and to recompense for Q at the system. The stator field-oriented VC is approved in the RSC , so long as effectual conduct of P and Q [35], [37], [38]. The winding arrangement of the asymmetrical induction machine (IM) is shown in Fig. 2 [39], [40]. The corresponding circuit illustration of an IM is given away in Fig. 3 and Fig. 4. In these Figures the IM is epitomized as a 2-Ø IM. For the modeling of DFIWG in d-q frame reference, the 2-Ø stator (d_s-q_s) and rotor (d_r-q_r) variables in a d-q frame are represented. The stator circuit formulas can be expressed as [41]-[44]:

$$V^s{}_{qs} = R_s\, I^s{}_{qs} + \frac{d}{dt}\psi^s{}_{qs} \tag{1}$$

$$V^s{}_{ds} = R_s\, I^s{}_{ds} + \frac{d}{dt}\psi^s{}_{ds} \tag{2}$$

where $\psi^s{}_{qs}$ and $\psi^s{}_{ds}$ are q-axis and d-axis stator flux linkages, respectively. When changing equation (1) and equation (2) to a d-q frame, the (3) and (4) is expressed as:

$$V_{qs} = R_s I_{qs} + \frac{d}{dt}\psi_{qs} + \omega_e \psi_{ds} \tag{3}$$

$$V_{ds} = R_s I_{ds} + \frac{d}{dt}\psi_{ds} - \omega_e \psi_{qs} \tag{4}$$

where all the variables are in a synchronously rotating frame. The bracketed terms are defined as the back e.m.f. When $\omega_e = 0$ the d and q axis is zero and the formulas change to stationary system. If $\omega_r = 0$, (5) and (6) are expressed as:

$$V_{qr} = R_r I_{qr} + \frac{d}{dt}\psi_{qr} + \omega_e \psi_{dr} \tag{5}$$

$$V_{dr} = R_r I_{dr} + \frac{d}{dt}\psi_{dr} - \omega_e \psi_{qr} \tag{6}$$

If the rotor rotates at ω_r, at that time the d-q axes static on the rotor dishonestly will change at ω_e-ω_r. Equations (7) and (8) are expressed by replacement ω_e-ω_r in position ω_e:

$$V_{qr} = R_r I_{qr} + \frac{d}{dt}\psi_{qr} + (\omega_e - \omega_r)\psi_{dr} \tag{7}$$

$$V_{dr} = R_r I_{dr} + \frac{d}{dt}\psi_{dr} - (\omega_e - \omega_r)\psi_{qr} \tag{8}$$

The ψ for rotor and stator is inferred from Fig. 3 and Fig. 4 in (9)-(14):

$$\psi_{qs} = L_{Is} i_{qs} + L_m\left(i_{qs} + i_{qr}\right) = L_s i_{qs} + L_m i_{qr} \tag{9}$$

$$\psi_{ds} = L_{Is} i_{ds} + L_m(i_{ds} + i_{dr}) = L_s i_{ds} + L_m i_{dr} \tag{10}$$

$$\psi_{qr} = L_{Ir} i_{qr} + L_m\left(i_{qs} + i_{qr}\right) = L_r i_{qr} + L_m i_{qs} \tag{11}$$

$$\psi_{dr} = L_{Ir} i_{dr} + L_m(i_{ds} + i_{dr}) = L_r i_{dr} + L_m i_{ds} \tag{12}$$

$$\psi_{qm} = L_m\left(i_{qs} + i_{qr}\right) \tag{13}$$

$$\psi_{dm} = L_m(i_{ds} + i_{dr}) \tag{14}$$

Equations (1)-(14) describe the complete electrical modeling of DFIWG. Whereas equation (15) couriers the relatives of mechanical variables. The ω_r is linked to the torque as:

$$T_e = T_1 + \mathrm{J}\frac{d\omega m}{dt} + \mathrm{B}\omega_m = T_1 + \frac{2}{p}\mathrm{J}\frac{d\omega r}{dt} + \frac{2}{p}\mathrm{B}\,\omega_m \tag{15}$$

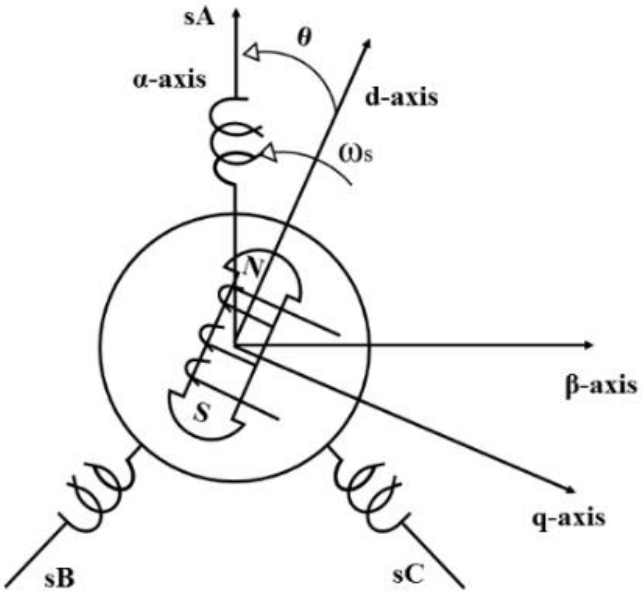

Fig. 2. dq-coordinate frame of the IM

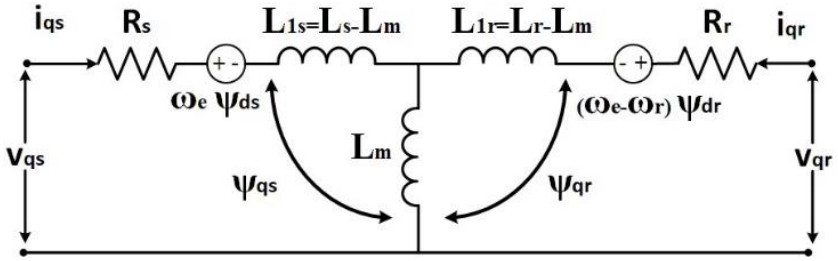

Fig. 3. Q-axis circuit of the DFIWG

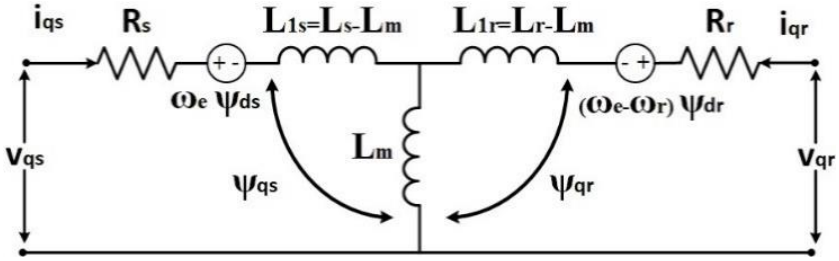

Fig. 4. D-axis circuit of the DFIWG

2.3. Control of DFIG

Fig. 5. displays the detailed control scheme of DFIWG [26]. The stator voltage vector angle (θ_s), and the rotor position angle (θ_r), angles are used to clarify the control process. The slip angle is identified by $\theta_{s1} = \theta_s - \theta_r$. The abc /dq and dq/abc transformation blocks are also utilized. The θ_s is obtained where V_{as}, V_{bs}, and V_{cs} are measured [45]-[47].

The optimal torque MPPT block generates the T^*_e. The i^*_{dr} is calculated according to equation (5). For a given Q^*_s the i^*_{qr} is calculated by equation (6). The i^*_{dr} and i^*_{qr} are then compared to the measured values, i_{dr} and i_{qr}, and the errors passed through PI controllers. The output of the PI controllers, v^*_{dr} and $v^*_{qr}$are transformed into v^*_{ar}, v^*_{br} and v^*_{cr} PWM block generates gating signals for the RSC. The GSC performs two main functions: (1) it keeps the DCLV constant, and (2) provides Q to the grid when required. The Q^*_{GSC} can be set to zero for the unity power factor (UPF) operation. The overall PF of the DFIWG is then controlled by the RSC through Q^*_s [48]-[50].

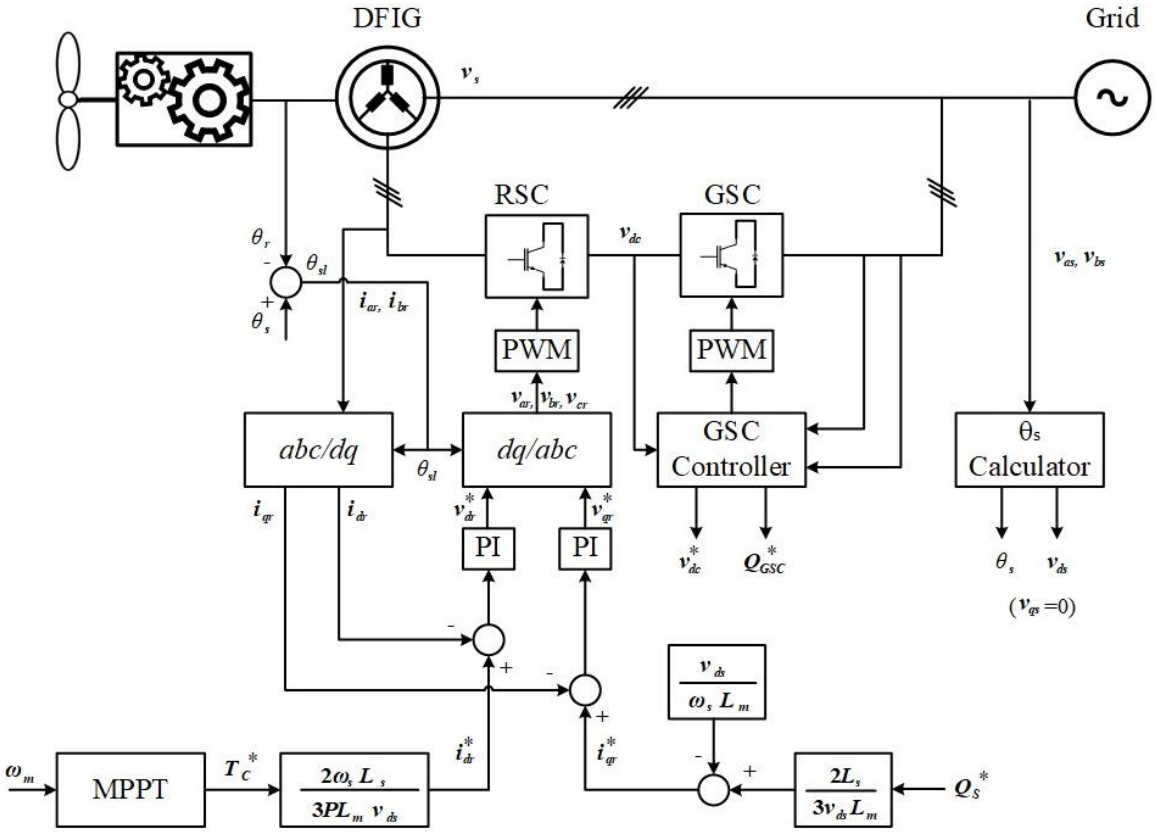

Fig. 5. Block diagram of a DFIWG with stator voltage-oriented control

2.4. Modelling of Crowbar

The crowbar action can often be represented as in (16). The parameters for each of the subsequent equations are explained in detail [51]-[53].

$$V_C = F_S \, R_C \, I_C \tag{16}$$

$$T_r{}^{SC} = \left(\frac{L_r{}^{SC}}{R_r + R_{\tau c}} \right) \tag{17}$$

$$I_r{}^{max} = \left(\frac{V_r{}^{max}}{\sqrt{(X_r{}^{sc})^2 + (R_{\tau c})^2}} \right) \tag{18}$$

$$R_{\tau c} < \left(\frac{\sqrt{2}\, X_{rs}{}^{sc} \, V_r{}^{max}}{\sqrt{3.2\,(V_s)^2 + 2(\,V_r{}^{max})^2}} \right) \tag{19}$$

$$V_r = k\, m\, V_{DC}\,, and\ k = \left(\frac{1}{\sqrt{3}} \right) \frac{V_{DC}{}^{b}}{V_r{}^{b}} \tag{20}$$

$$V_r{}^{max} = IR_{DC} - V_{DC} = 0 \tag{21}$$

2.5. Modelling of STATCOM

The STATCOM (shunt reactive compensator) can either generate or absorb reactive power. In a three-phase configuration, the following equations are used to represent STATCOM and fully discussed in [54], [55]:

$$L\frac{d_{ia}}{dt}=-RI_a+(V_a-V_{a1}) \quad (22)$$

$$L\frac{d_{ib}}{dt}=-RI_b+(V_b-V_{b1}) \quad (23)$$

$$L\frac{d_{ic}}{dt}=-RI_c+(V_c-V_{c1}) \quad (24)$$

$$L\frac{d_{id}}{dt}=-RI_d+\omega LI_q(V_d-V_{d1}) \quad (25)$$

$$L\frac{d_{iq}}{dt}=-RI_q+\omega LI_d\left(V_q-V_{q1}\right) \quad (26)$$

$$V_{d1}=KmV_{dc}\sin(\delta) \quad (27)$$

$$V_{q1}=KmV_{dc}\cos(\delta) \quad (28)$$

$$m=\frac{\sqrt{V_{d1}^2+V_{q1}^2}}{km} \quad (29)$$

$$\delta=\tan^{-1}\frac{V_{q1}}{V_{d1}} \quad (30)$$

$$P_{ac}=1.5\left(V_dI_d+V_qI_q\right)=0 \quad (31)$$

$$Q_{ac}=1.5\left(V_dI_q-V_qI_d\right) \quad (32)$$

3. Simulation Results and Discussion

Simulation has been done on a 1.5 MW,575 V, 60 Hz, 3poles DFIWG by using MATLAB/Simulink [10], [56]. Studying DFIWG performance includes the time response of p, Q, V_{DC}, V_{ABC}, and I_{ABC} during normal and abnormal conditions like symmetrical and asymmetrical faults. Crowbar and STATCOM devices are used for enhancing the performance of DFIWG, and their connections are illustrated in Fig. 6 and Fig. 7. The DFIWG parameters are listed in Table 1.

Table 1. DFIWG data

DFIWG Parameters	Value
Rated power	1.5 MW
Rated stator voltage	575 V
Rated frequency	60 Hz
DC-Link voltage	1150 V
Pole pairs	3
Stator resistance	0.023 pu
Rotor leakage inductance	0.16 pu
Mutual inductance	2.9 pu
Stator leakage inductance	0.18 pu
Rotor resistance	0.016 pu
Inertia constant	0.685 pu

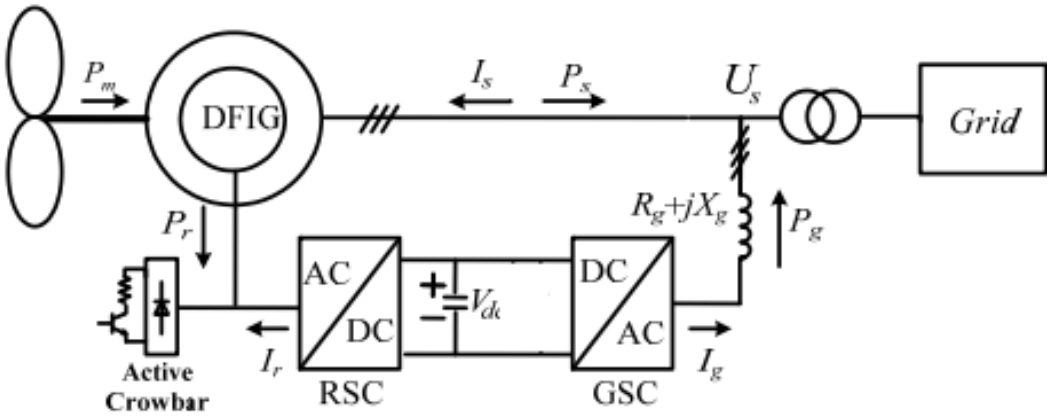

Fig. 6. Schematic diagram of crowbar connected to DFIWG [57]

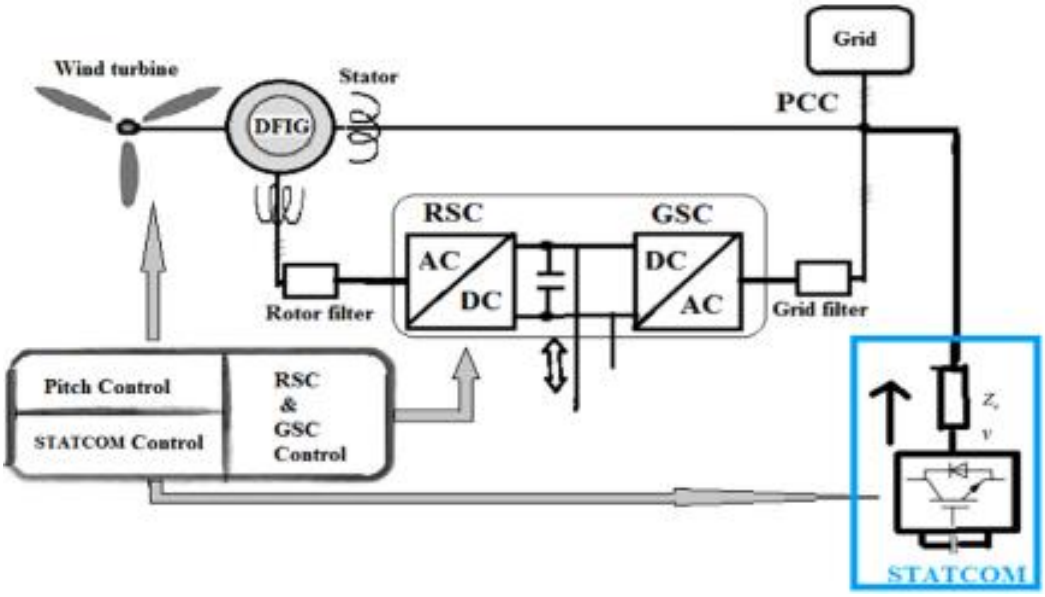

Fig. 7. Schematic diagram of STATCOM connected to DFIWG [58]

3.1. Studying the Dynamic Performance of DFIWG During Starting

Fig. 8 from (a) to (e) shows the performance of grid-connected DFIWG in the case of balanced grid operation. Set point P=1.5 MW and Q=0 which means that DFIWG is operated at UPF. The DCLV is maintained constant at 1150 V. The system voltage is 1 pu during the time simulation as in Fig. 8 (a). Some overshoot happens in the rest of the presented parameters. Results show that both STATCOM and crowbar enhanced the dynamic performance of DFIWG under this situation.

3.2. Studying the Dynamic Performance of DFIWG Under Three Phases to Ground Fault (3ØGF)

Dynamic performance of the system is studied with crowbar and STATCOM under 3ØGF. The most severe fault is this sort which leads to the voltage decreased to zero roughly. In this paper assumption of grid disturbance occurs at t=0.25 seconds and cleared at 0.3 seconds as seen in Fig. 9 (a). During the fault period, the P decreased to zero and after fault clearing, the P returned to its rated value of 1.5 MW as seen in Fig. 9 (b), but Q drawn from the grid increased during the fault period which reached 1Mvar roughly and after fault clearing Q returns to its rated value 0 as seen in Fig. 9 (c). The V_{DC} increased during the fault period to reach 1800 V, but with a crowbar and STATCOM decreased to reach 1268 V only that is protecting the BTBC from damage as seen in Fig. 9 (d). Fig. 9 (e) depicts the injected current to the grid. Fig. 9 proves that both STATCOM and crowbar have

superior performance compared to the base case in this event. The DFIWG with the investigated tools achieves FRTC and keeps the V_{DC} below permissible limits.

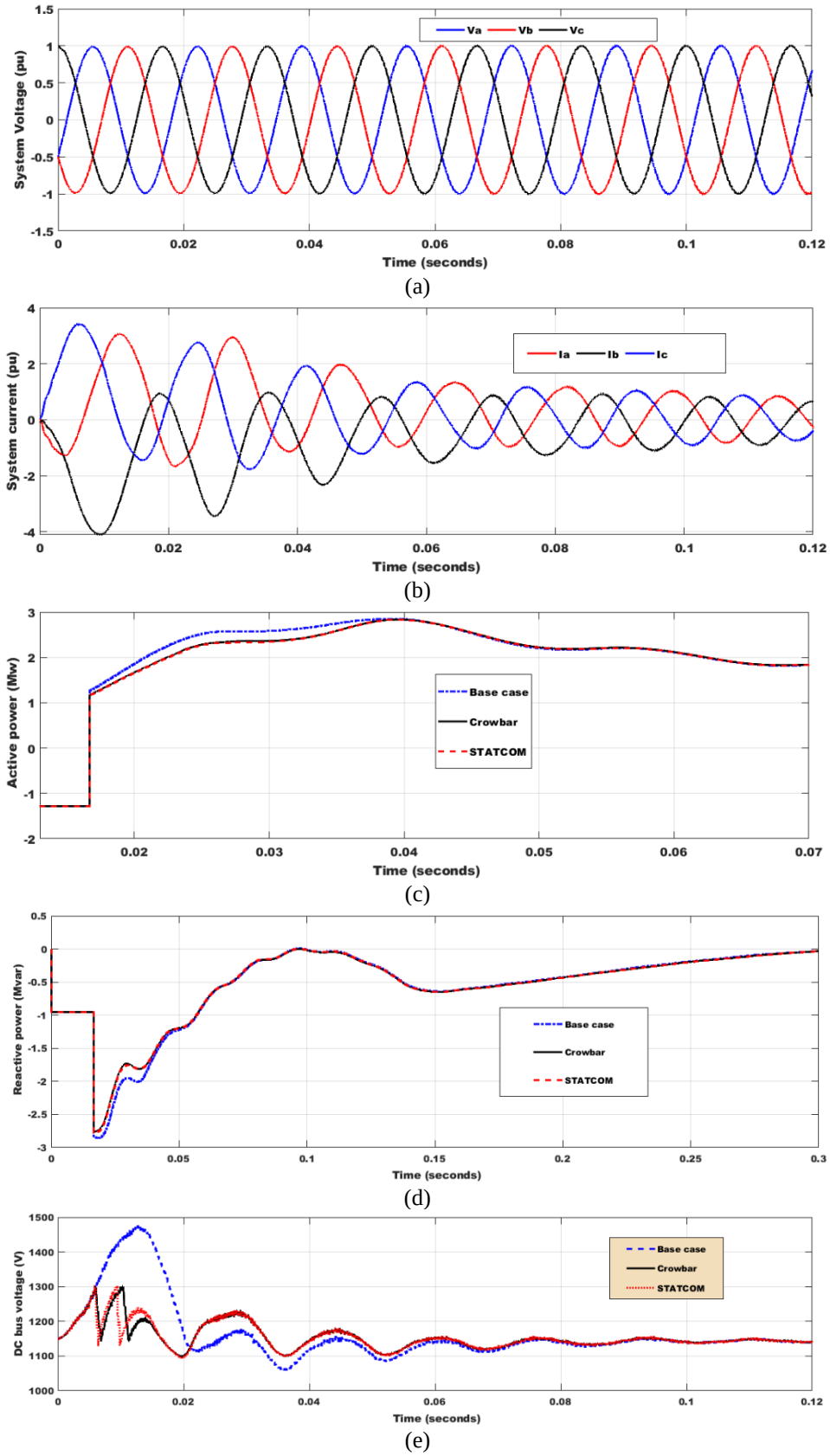

Fig. 8. Simulation results during normal operation: (a) V_{ABC}, (b) I_{ABC}, (c) P, (d) Q, (e) V_{DC}

3.3. Studying the Dynamic Performance of DFIWG Under the Double Line to Ground Fault (2ØGF)

At the occurrence of the 2ØGF the system voltage changes as depicted in Fig. 10 (a). The P drops to nearly 0.5 MW with a crowbar and reaches 0.62 MW with STATCOM as shown in Fig. 10 (b). The DFIWG absorbs about 1Mvar during the fault period but STATCOM gives the highest Q to support the system voltage as depicted in Fig. 10 (c). The V_{DC} reaches about 1330 V in the base case and reaches 1250 V with STATCOM but with the crowbar reaches 1200 V as depicted in Fig. 10 (d). Fig. 9 (e) depicts the injected current to the grid. Fig. 10 proves that both STATCOM and crowbar have superior performance compared to the base case in this event. The DFIWG with the investigated tools achieves FRTC and keeps the V_{DC} below permissible limits.

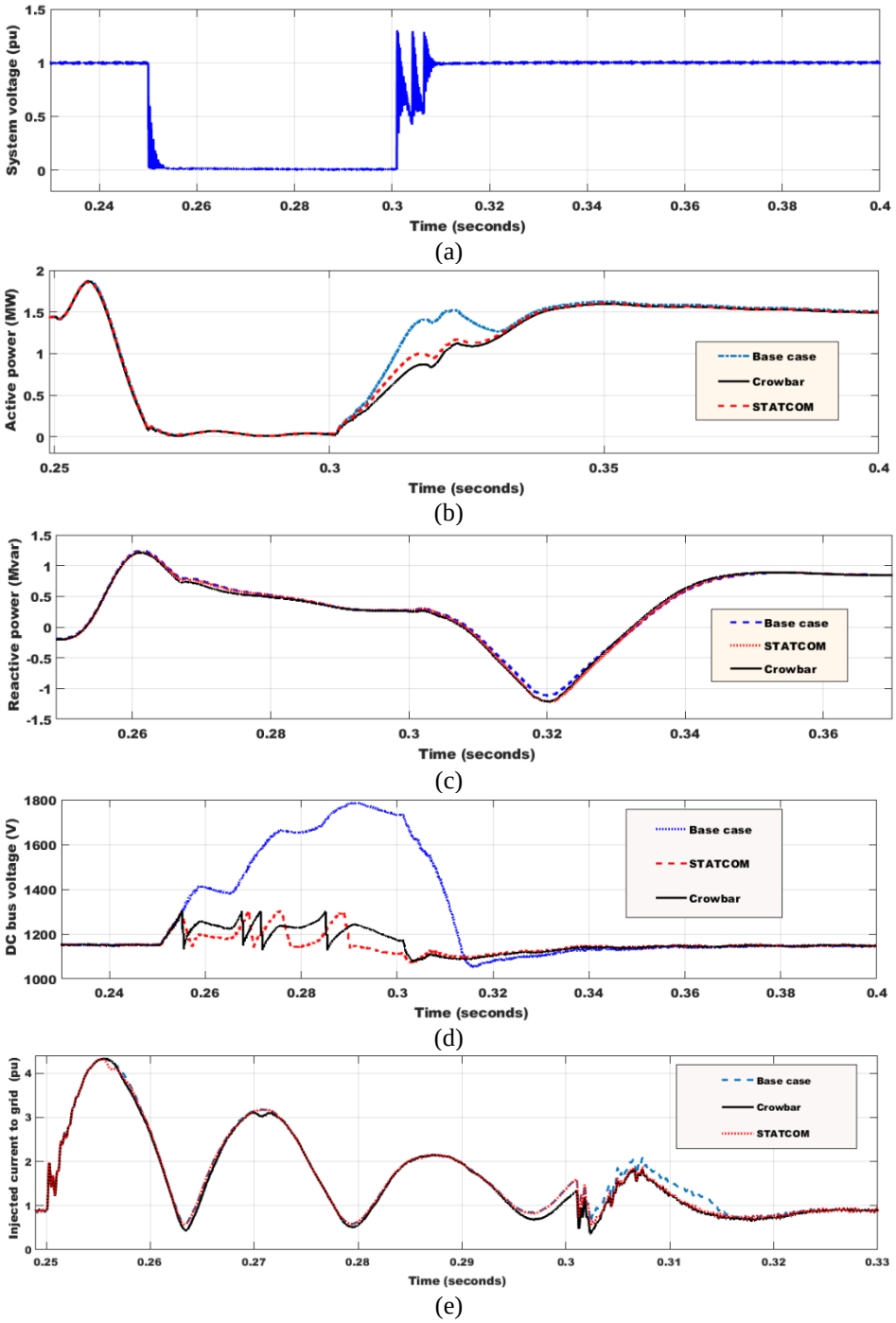

Fig. 9. Simulation results under 3ØGF: (a) system voltage, (b) P, (c) Q, (d) grid current, (e) V_{DC}

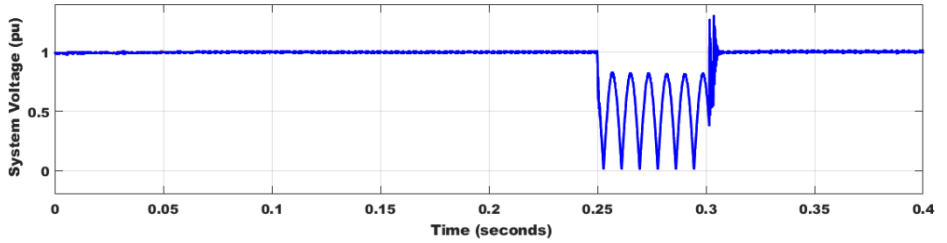

(a)

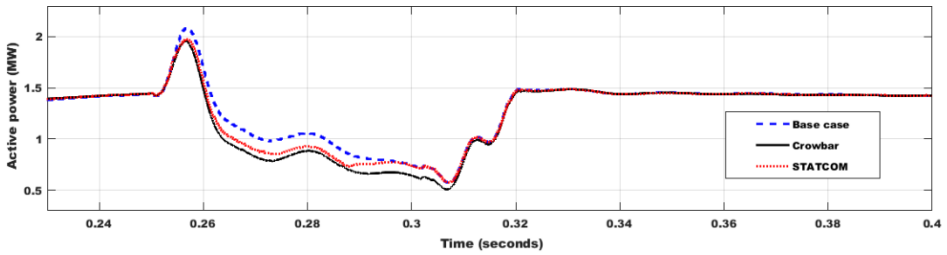

(b)

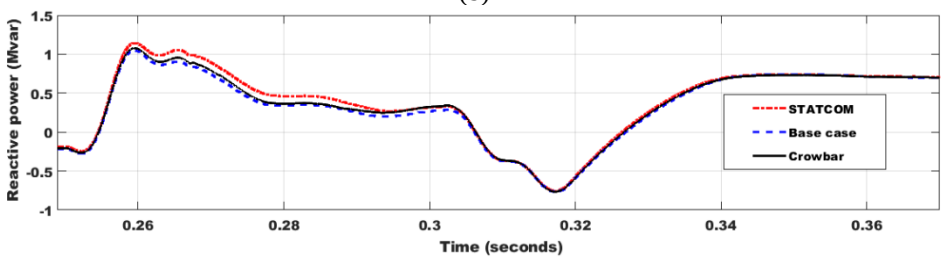

(c)

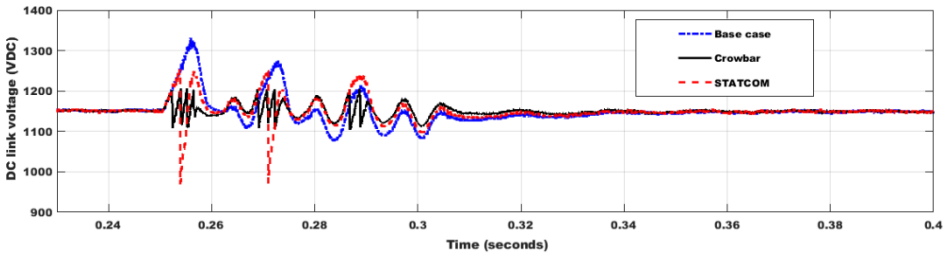

(d)

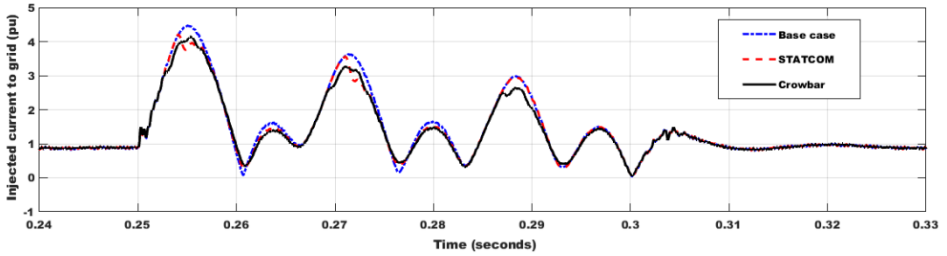

(e)

Fig. 10. Simulation results under 2ØGF: (a) system voltage, (b) P, (c) Q, (d) grid current, (e) V_{DC}

4. Conclusions

When failures occur, DFIWG is under a lot of stress. By using a crowbar and STATCOM, DFIWG may remain connected to the grid and restrict currents and voltages below predetermined thresholds. Q regulation cannot be provided by DFIWG equipped with a crowbar, although it can withstand grid disturbances, according to simulations. Investigations are conducted into the use of a STATCOM linked to a DFIWG to enable uninterruptible FRTC of GV faults. Whereas the DFIWG can carry on with its nominal operation and satisfy any grid code requirement without requiring additional protective mechanisms, the STATCOM can make up for the defective line voltage.

Simulation results declared that the voltage dip in the grid leads to overvoltage in the DC link, over-currents in DFIWG winding, and a decrease in active power. From the previous discussion, we find that the DFIWG connected to the utility grid gave a better dynamic performance with the STATCOM tool in case of a three-phase fault and double line to ground fault compared to an active crowbar. Active crowbar and STATCOM tools have succeeded in enhancing the machine's performance.

Author Contribution: All authors contributed equally to the main contributor to this paper. All authors read and approved the final paper.

Data Availability: The data used to support the findings of this study are available at reasonable request from the corresponding author.

Conflicts of Interest: The authors declare that they have no conflicts of interest.

Acknowledgment: The authors extend their appreciation to Prince Sattam bin Abdulaziz University for funding this research work through the project number (PSAU/2024/01/29320).

References

[1] P. Cheng and H. Nian, "Collaborative Control of DFIG System During Network Unbalance Using Reduced-Order Generalized Integrators," *IEEE Transactions on Energy Conversion*, vol. 30, no. 2, pp. 453-464, 2015, https://doi.org/10.1109/TEC.2014.2363671.

[2] M. N. A. Hamid *et al*., "Adaptive Frequency Control of an Isolated Microgrids Implementing Different Recent Optimization Techniques," *International Journal of Robotics and Control Systems*, vol. 4, no. 3, pp. 1000-1012, 2024, https://doi.org/10.31763/ijrcs.v4i3.1432.

[3] F. Menzri, T. Boutabba, I. Benlaloui, H. Bawayan, M. I. Mosaad, and M. M. Mahmoud, "Applications of hybrid SMC and FLC for augmentation of MPPT method in a wind-PV-battery configuration," *Wind Engineering*, 2024, https://doi.org/10.1177/0309524X241254364.

[4] B. S. Atia *et al*., "Applications of Kepler Algorithm-Based Controller for DC Chopper: Towards Stabilizing Wind Driven PMSGs under Nonstandard Voltages," *Sustainability*, vol. 16, no. 7, p. 2952, 2024, https://doi.org/10.3390/su16072952.

[5] Z. Hao, Z. Fuhong, Z. Hao, G. Ziming, G. Ziping, "Study on Regulation and Control of Active Wind Power Fluctuations," *Information Technology Journal*, vol. 13, no. 18, pp. 2743-2748, 2014, https://doi.org/10.3923/itj.2014.2743.2748.

[6] M. M. Mahmoud *et al*., "Evaluation and Comparison of Different Methods for Improving Fault Ride-Through Capability in Grid-Tied Permanent Magnet Synchronous Wind Generators," *International Transactions on Electrical Energy Systems*, vol. 2023, no. 1, pp. 1-22, 2023, https://doi.org/10.1155/2023/7717070.

[7] S. R. K. Joga *et al*., "Applications of tunable-Q factor wavelet transform and AdaBoost classier for identification of high impedance faults: Towards the reliability of electrical distribution systems," *Energy Exploration & Exploitation*, 2024, https://doi.org/10.1177/01445987241260949.

[8] H. Alnami, S. A. E. M. Ardjoun, and M. M. Mahmoud, "Design, implementation, and experimental validation of a new low-cost sensorless wind turbine emulator: Applications for small-scale turbines," *Wind Engineering*, 2024, https://doi.org/10.1177/0309524X231225776.

[9] Y. Moumani, A. J. Laafou, and A. A. Madi, "A comparative study based on proportional integral and backstepping controllers for doubly fed induction generator used in wind energy conversion system," *Archives of Electrical Engineering*, vol. 72, no. 1, pp. 211-228, 2023, https://doi.org/10.24425/aee.2023.143698.

[10] M. M. Mahmoud, B. S. Atia, A. Y. Abdelaziz, and N. A. N. Aldin, "Dynamic Performance Assessment of PMSG and DFIG-Based WECS with the Support of Manta Ray Foraging Optimizer Considering MPPT, Pitch Control, and FRT Capability Issues," *Processes*, vol. 12, no. 10, p. 2723, 2022, https://doi.org/10.3390/pr10122723.

[11] M. Awad *et al*., "A review of water electrolysis for green hydrogen generation considering PV/wind/hybrid/hydropower/geothermal/tidal and wave/biogas energy systems, economic analysis, and its application," *Alexandria Engineering Journal*, vol. 87, pp. 213-239, 2024, https://doi.org/10.1016/j.aej.2023.12.032.

[12] E. Tremblay, S. Atayde and A. Chandra, "Comparative Study of Control Strategies for the Doubly Fed Induction Generator in Wind Energy Conversion Systems: A DSP-Based Implementation Approach," *IEEE Transactions on Sustainable Energy*, vol. 2, no. 3, pp. 288-299, 2011, https://doi.org/10.1109/TSTE.2011.2113381.

[13] I. E. Maysse *et al*., "Nonlinear Observer-Based Controller Design for VSC-Based HVDC Transmission Systems Under Uncertainties," *IEEE Access*, vol. 11, pp. 124014-124030, 2023, https://doi.org/10.1109/ACCESS.2023.3330440.

[14] H. A. Aroussi, E. Ziani, M. Bouderbala, and B. Bossoufi, "Enhancement of the direct power control applied to DFIG-WECS," *International Journal of Electrical and Computer Engineering*, vol. 10, no. 1, pp. 35-46, 2020, http://doi.org/10.11591/ijece.v10i1.pp35-46.

[15] J. S. Solís-Chaves, M. S. Barreto, M. B. C. Salles, V. M. Lira, R. V. Jacomini, and A. J. Sguarezi Filho, "A direct power control for DFIG under a three phase symmetrical voltage sag condition," *Control Engineering Practice*, vol. 65, pp. 48-58, 2017, https://doi.org/10.1016/j.conengprac.2017.05.002.

[16] E. G. Shehata, "Active and reactive power control of doubly fed induction generators for wind energy generation under unbalanced grid voltage conditions," *Electric Power Components and Systems*, vol. 41, no. 6, pp. 619-640, 2013, https://doi.org/10.1080/15325008.2013.763308.

[17] K. Roummani *et al*., "A new concept in direct-driven vertical axis wind energy conversion system under real wind speed with robust stator power control," *Renewable Energy*, vol. 143, pp. 478-487, 2019, https://doi.org/10.1016/j.renene.2019.04.156.

[18] F. Valenciaga, R. D. Fernández, and F. Inthamoussou, "A second order sliding power control & resonant filtering approach to mitigate grid unbalance effects on a DOIG wind energy based system," *International Conference on Renewable Energies and Power Quality*, vol. 1, no. 15, pp. 255-260, 2017, https://doi.org/10.24084/repqj15.286.

[19] Y. Zhang, J. Jiao and D. Xu, "Direct Power Control of Doubly Fed Induction Generator Using Extended Power Theory Under Unbalanced Network," *IEEE Transactions on Power Electronics*, vol. 34, no. 12, pp. 12024-12037, 2019, https://doi.org/10.1109/TPEL.2019.2906013.

[20] S. Tohidi and M. I. Behnam, "A comprehensive review of low voltage ride through of doubly fed induction wind generators," *Renewable and Sustainable Energy Reviews*, vol. 57, pp. 412-419, 2016, https://doi.org/10.1016/j.rser.2015.12.155.

[21] S. Gao, H. Zhao, Y. Gui, D. Zhou, V. Terzija and F. Blaabjerg, "A Novel Direct Power Control for DFIG With Parallel Compensator Under Unbalanced Grid Condition," *IEEE Transactions on Industrial Electronics*, vol. 68, no. 10, pp. 9607-9618, 2021, https://doi.org/10.1109/TIE.2020.3022495.

[22] H. Benbouhenni, F. Mehedi, and L. Soufiane, "New direct power synergetic-SMC technique based PWM for DFIG integrated to a variable speed dual-rotor wind power," *Automatika*, vol. 63, no. 4, pp. 718-731, 2022, https://doi.org/10.1080/00051144.2022.2065801.

[23] Y. Zhang, J. Jiao, D. Xu, D. Jiang, Z. Wang and C. Tong, "Model Predictive Direct Power Control of Doubly Fed Induction Generators Under Balanced and Unbalanced Network Conditions," *IEEE Transactions on Industry Applications*, vol. 56, no. 1, pp. 771-786, 2020, https://doi.org/10.1109/TIA.2019.2947396.

[24] C. Cheng, P. Cheng, H. Nian, and D. Sun, "Model predictive stator current control of doubly fed induction generator during network unbalance," *IET Power Electronics*, vol. 11, no. 1, pp. 120-128, 2018, https://doi.org/10.1049/iet-pel.2017.0049.

[25] X. Ran, B. Xu, K. Liu and J. Zhang, "An Improved Low-Complexity Model Predictive Direct Power Control With Reduced Power Ripples Under Unbalanced Grid Conditions," *IEEE Transactions on Power Electronics*, vol. 37, no. 5, pp. 5224-5234, 2022, https://doi.org/10.1109/TPEL.2021.3131794.

[26] Y. El Karkri, A. B. Rey-Boué, H. El Moussaoui, J. Stöckl, and T. I. Strasser, "Improved control of grid-connected DFIG-based wind turbine using proportional-resonant regulators during unbalanced grid," *Energies*, vol. 12, no. 21, p. 4041, 2019, https://doi.org/10.3390/en12214041.

[27] M. M. Mahmoud, "Improved current control loops in wind side converter with the support of wild horse optimizer for enhancing the dynamic performance of PMSG-based wind generation system," *International Journal of Modelling and Simulation*, vol. 43, no. 6, pp. 952-966, 2023, https://doi.org/10.1080/02286203.2022.2139128.

[28] H. Chojaa *et al*., "Nonlinear Control Strategies for Enhancing the Performance of DFIG-Based WECS under a Real Wind Profile," *Energies*, vol. 15, no. 18, p. 6650, 2022, https://doi.org/10.3390/en15186650.

[29] M. Wu, L. Ding, C. Xue and Y. W. Li, "Model-Based Closed-Loop Control for High-Power Current Source Rectifiers Under Selective Harmonic Elimination/Compensation PWM With Fast Dynamics," *IEEE Journal of Emerging and Selected Topics in Power Electronics*, vol. 10, no. 5, pp. 5921-5932, 2022, https://doi.org/10.1109/JESTPE.2022.3152494.

[30] C. Liu, W. Chen, F. Blaabjerg and D. Xu, "Optimized design of resonant controller for stator current harmonic compensation in DFIG wind turbine systems," *2012 Twenty-Seventh Annual IEEE Applied Power Electronics Conference and Exposition (APEC)*, pp. 2038-2044, 2012, https://doi.org/10.1109/APEC.2012.6166102.

[31] Z. Zheng, G. Yang, and H. Geng, "Coordinated control of a doubly-fed induction generator-based wind farm and a static synchronous compensator for low voltage ride-through grid code compliance during asymmetrical grid faults," *Energies*, vol. 6, no. 9, pp. 4660-4681, 2013, https://doi.org/10.3390/en6094660.

[32] N. F. Ibrahim *et al*., "Multiport Converter Utility Interface with a High-Frequency Link for Interfacing Clean Energy Sources (PV\Wind\Fuel Cell) and Battery to the Power System: Application of the HHA Algorithm," *Sustainability*, vol. 15, no. 18, p. 13716, 2023, https://doi.org/10.3390/su151813716.

[33] H. Boudjemai *et al*., "Experimental Analysis of a New Low Power Wind Turbine Emulator Using a DC Machine and Advanced Method for Maximum Wind Power Capture," *IEEE Access*, vol. 11, pp. 92225-92241, 2023, https://doi.org/10.1109/ACCESS.2023.3308040.

[34] M. E. B. Aguilar, D. V. Coury, R. Reginatto, R. M. Monaro, P. T. de Godoy, and T. G. Jahn, "Multi-Objective PSO for Control-Loop Tuning of DFIG Wind Turbines with Chopper Protection and Reactive-Current Injection," *Energies*, vol. 17, no. 1, p. 28, 2024, https://doi.org/10.3390/en17010028.

[35] A. A. Chhipą *et al*., "Modeling and Control Strategy of Wind Energy Conversion System with Grid-Connected Doubly-Fed Induction Generator," *Energies*, vol. 15, no. 18, p. 6694, 2022, https://doi.org/10.3390/en15186694.

[36] M. Awad, M. M. Mahmoud, Z. M. S. Elbarbary, L. Mohamed Ali, S. N. Fahmy, and A. I. Omar, "Design and analysis of photovoltaic/wind operations at MPPT for hydrogen production using a PEM electrolyzer: Towards innovations in green technology," *PLoS One*, vol. 18, no. 7, p. e0287772, 2023, https://doi.org/10.1371/journal.pone.0287772.

[37] M. M. Mahmoud, M. K. Ratib, M. M. Aly, A. Moamen, and M. A. Rahim, "Effect of Grid Faults on Dominant Wind Generators for Electric Power System Integration: A Comparison and Assessment," *Energy Systems Research*, vol. 4, no. 3, pp. 70–78, 2021, https://doi.org/10.3390/axioms12050420.

[38] M. M. Mahmoud et al., "Application of Whale Optimization Algorithm Based FOPI Controllers for STATCOM and UPQC to Mitigate Harmonics and Voltage Instability in Modern Distribution Power Grids," *Axioms*, vol. 12, no. 5, p. 420, 2023, https://doi.org/10.3390/axioms12050420.

[39] B. Yang, L. Jiang, L. Wang, W. Yao, and Q. H. Wu, "Nonlinear maximum power point tracking control and modal analysis of DFIG based wind turbine," *International Journal of Electrical Power & Energy Systems*, vol. 74, pp. 429-436, 2016, https://doi.org/10.1016/j.ijepes.2015.07.036.

[40] S. Gupta and A. Shukla, "Improved dynamic modelling of DFIG driven wind turbine with algorithm for optimal sharing of reactive power between converters," *Sustainable Energy Technologies and Assessments*, vol. 51, p. 101961, 2022, https://doi.org/10.1016/j.seta.2022.101961.

[41] A. H. Elmetwaly *et al*., "Modeling, Simulation, and Experimental Validation of a Novel MPPT for Hybrid Renewable Sources Integrated with UPQC: An Application of Jellyfish Search Optimizer," *Sustainability*, vol. 15, no. 6, p. 5209, 2023, https://doi.org/10.3390/su15065209.

[42] O. M. Kamel, A. A. Z. Diab, M. M. Mahmoud, A. S. Al-Sumaiti, and H. M. Sultan, "Performance Enhancement of an Islanded Microgrid with the Support of Electrical Vehicle and STATCOM Systems," *Energies*, vol. 16, no. 4, p. 1577, 2023, https://doi.org/10.3390/en16041577.

[43] H. Boudjemai *et al*., "Application of a Novel Synergetic Control for Optimal Power Extraction of a Small-Scale Wind Generation System with Variable Loads and Wind Speeds," *Symmetry*, vol. 15, no. 2, p. 369, 2023, https://doi.org/10.3390/sym15020369.

[44] M. M. Mahmoud *et al*., "Voltage Quality Enhancement of Low-Voltage Smart Distribution System Using Robust and Optimized DVR Controllers: Application of the Harris Hawks Algorithm," *International Transactions Electrical Energy Systems*, vol. 2022, no. 1, pp. 1-18, 2022, https://doi.org/10.1155/2022/4242996.

[45] F. E. V. Taveiros, L. S. Barros, and F. B. Costa, "Back-to-back converter state-feedback control of DFIG (doubly-fed induction generator)-based wind turbines," *Energy*, vol. 89, pp. 896-906, 2015, https://doi.org/10.1016/j.energy.2015.06.027.

[46] A. A. Ansari, G. Dyanamina and A. A. Ansari, "Decoupled Control of Rotor Side Power Electronic Converter for Grid Connected DFIG Based Wind Energy System," *2023 IEEE International Students' Conference on Electrical, Electronics and Computer Science (SCEECS)*, pp. 1-6, 2023, https://doi.org/10.1109/SCEECS57921.2023.10063093.

[47] N. A. N. Aldin, W. S. E. Abdellatif, Z. M. S. Elbarbary, A. I. Omar and M. M. Mahmoud, "Robust Speed Controller for PMSG Wind System Based on Harris Hawks Optimization via Wind Speed Estimation: A Real Case Study," *IEEE Access*, vol. 11, pp. 5929-5943, 2023, https://doi.org/10.1109/ACCESS.2023.3234996.

[48] M. Soomro *et al*., "Performance Improvement of Grid-Integrated Doubly Fed Induction Generator under Asymmetrical and Symmetrical Faults," *Energies*, vol. 16, no. 8, p. 3350, 2023, https://doi.org/10.3390/en16083350.

[49] K. Sabzevari *et al*., "Low-voltage ride-through capability in a DFIG using FO-PID and RCO techniques under symmetrical and asymmetrical faults," *Science Reports*, vol. 13, no. 17534, 2023, https://doi.org/10.1038/s41598-023-44332-y.

[50] R. Sitharthan, C. K. Sundarabalan, K. R. Devabalaji, S. K. Nataraj, and M. Karthikeyan, "Improved fault ride through capability of DFIG-wind turbines using customized dynamic voltage restorer," *Sustainable Cities and Society*, vol. 39, pp. 114-125, 2018, https://doi.org/10.1016/j.scs.2018.02.008.

[51] A. M. A. Haidar, K. M. Muttaqi and M. T. Hagh, "A Coordinated Control Approach for DC link and Rotor Crowbars to Improve Fault Ride-Through of DFIG-Based Wind Turbine," *IEEE Transactions on Industry Applications*, vol. 53, no. 4, pp. 4073-4086, 2017, https://doi.org/10.1109/TIA.2017.2686341.

[52] Y. Ling, "A fault ride through scheme for doubly fed induction generator wind turbine," *Australian Journal of Electrical and Electronics Engineering*, vol. 15, no. 3, pp. 71-79, 2018, https://doi.org/10.1080/1448837X.2018.1525172.

[53] J. Yin, X. Huang, and W. Qian, "Analysis and research on short-circuit current characteristics and grid access faults of wind farms with multi-type fans," *Energy Reports*, vol. 11, pp. 1161-1170, 2024, https://doi.org/10.1016/j.egyr.2023.12.046.

[54] A. F. Abdou, H. R. Pota, A. Abu-Siada and Y. M. Alharbi, "Application of STATCOM-HTS to improve DFIG performance and FRT during IGBT short circuit," *2014 Australasian Universities Power Engineering Conference (AUPEC)*, pp. 1-5, 2014, https://doi.org/10.1109/AUPEC.2014.6966641.

[55] M. M. Mahmoud *et al*., "Integration of Wind Systems with SVC and STATCOM during Various Events to Achieve FRT Capability and Voltage Stability: Towards the Reliability of Modern Power Systems," *International Journal of Energy Research*, vol. 2023, no. 1, pp. 1-28, 2023, https://doi.org/10.1155/2023/8738460.

[56] M. M. Mahmoud, M. Khalid Ratib, M. M. Aly, and A. M. M. Abdel-Rahim, "Wind-driven permanent magnet synchronous generators connected to a power grid: Existing perspective and future aspects," *Wind Engineering*, vol. 46, no. 1, pp. 189-199, 2022, https://doi.org/10.1177/0309524X211022728.

[57] Z. Wu, C. Zhu, and M. Hu, "Improved control strategy for DFIG wind turbines for low voltage ride through," *Energies*, vol. 6, no. 3, pp. 1181-1197, 2013, https://doi.org/10.3390/en6031181.

[58] D. V. N. Ananth and G. V. Nagesh Kumar, "Fault ride-through enhancement using an enhanced field oriented control technique for converters of grid connected DFIG and STATCOM for different types of faults," *ISA Transactions*, vol. 62, pp. 2-18, 2016, https://doi.org/10.1016/j.isatra.2015.02.014.